Received: 28 May 2024 | Revised: 16 July 2024 | Accepted: 20 August 2024 | Published online: 4 September 2024

RESEARCH ARTICLE

Archives of Advanced Engineering Science
2026, Vol. 4(2) 171–179
DOI: 10.47852/bonviewAAES42023514

BON VIEW PUBLISHING

Synthesis of Thermoelectric Nanocomposites by Incorporating Reduced Graphene Oxide

Jyoti Bhattacharjee[1] **and Subhasis Roy**[1,*]

[1]*Department of Chemical Engineering, University of Calcutta, India*

Abstract: Thermoelectric energy conversion technology is advancing by leveraging the Seebeck effect to transform waste heat into electricity. Oxide-based thermoelectric materials are particularly attractive due to their excellent figure of merit, chemical and thermal stability, and improved safety compared to chalcogenides. Despite numerous reported high-ZT oxides (ZT > 1), maintaining their stability at high temperatures remains a significant challenge. The sequential process involves blending the precursor materials, dissolving them in a solvent, and reacting them to form thermoelectric composites. RGO-doped bismuth titanate nanoparticles were characterized using X-ray diffraction and field emission scanning electron microscopy. We successfully synthesized high-ZT-doped n-type and Ag_2Te (p-type) nanostructures via a sol-gel method, achieving uniform microstructures with desirable thermoelectric properties. Ethylene glycol-based graphene was employed as an eco-friendly reducing agent. The synthesis method for nanomaterials incorporating reduced graphene oxide (rGO) as a dopant demonstrated an impressive Seebeck coefficient (S), a notable figure of merit, high carrier mobility (μ), and a promising power factor. RGO-doped bismuth telluride and Ag_2Te thin films were deposited onto FTO glass substrates via spin coating for p-type and n-type thermoelectric materials. This research revealed a figure of merit around $1.8*10^{-4}K^{-1}$ within the 800–900 K temperature range.

Keywords: composites, thermal conductivity, thermoelectric, Seebeck coefficient, figure of merit, power factor

1. Introduction

The Seebeck effect has led to considerable interest in thermoelectric (TE) energy conversion technology due to its ability to transform waste heat into electricity. Equation (1) primarily determines the efficiency of this conversion process through the TE figure of merit (ZT) [1, 2]:

$$ZT(= S^2 \cdot \sigma \cdot T \cdot \kappa^{-1}) \quad (1)$$

where S is the thermopower or Seebeck coefficient, σ is the electrical conductivity, T represents the absolute temperature, and κ is the total thermal conductivity of the TE materials [1]. When exposed to a temperature gradient, certain materials can convert heat directly into electricity, making them valuable for power generation from waste heat in remote areas [1, 2]. Currently, the most advanced TE materials are primarily composed of inorganic alloys based on Tellurium, which are suitable for use at low temperatures (<400°C). However, these materials are often brittle, dense, and costly. To address these challenges, researchers are exploring alternative materials like nanocarbon (e.g., carbon nanotubes or graphene), conducting polymers, and their composites [3, 4]. These organic materials offer flexibility and durability but struggle at temperatures above 300°C [4]. Incorporating reduced graphene oxide (rGO) as a dopant or component in TE materials offers several benefits, including enhanced electrical conductivity, reduced thermal conductivity (κ), tunable properties, and environmental friendliness [4]. Current research is focused on developing rGO-doped TE materials with improved efficiency and practical applications. These materials hold promise for waste heat recovery, power generation from temperature differences, and other energy conversion technologies [3, 4].

Despite significant progress, these materials' commercial and widespread application is still in the developmental stages, requiring further research to optimize them for real-world use [4, 5]. The efficiency of converting temperature differences into electrical power is largely determined by the TE ZT.

Several parameters, including the Seebeck coefficient, electrical conductivity, absolute temperature, and total κ of TE materials, influence the ZT [5, 6]. Since 2000, extensive efforts have been made to develop TE materials with high ZT values. Notable TE materials include lead chalcogenides, skutterudites, half-Heuslers, alloys, and tin selenide (SnSe) [5–7]. Through non-equilibrium processing techniques, an impressive TE ZT of approximately 2.5 was achieved at 650°C in the PbTe-SrTe system [8, 9]. Recent developments have removed performance-impairing tin oxides, allowing hole-doped SnSe polycrystalline samples to attain an even higher ZT of 3.1 at 510°C [4]. However, despite these advancements, the practical application of TE materials remains limited due to the high cost of rare elements and the scarcity of resources such as tellurium, which is particularly rare. Additionally, many commonly used materials, such as sulfides, selenides, and tellurides, pose toxicity issues [5]. Enhancing ZT often involves doping and altering material dimensionality through nanostructuring and nanocomposite. However, improving TE performance is challenging due to the complex relationship between electrical properties, where increasing carrier concentration (n) enhances the

***Corresponding author:** Subhasis Roy, Department of Chemical Engineering, University of Calcutta, India. Email: subhasis1093@gmail.com

power factor (PF). Research on reduced graphene-doped titanium dioxide nanocomposites aims to advance applications in photocatalysis, photovoltaics, and TEs [6, 8]. Metal oxides generally offer good chemical and thermal stability in air. They are safer than chalcogenide-based TE materials, making them promising candidates for high-ZT oxide-based TE materials.

Graphene has attracted significant attention over the last decade due to its unique optical and electrical properties. Its 2D hexagonal honeycomb structure provides exceptional electron mobility, a large specific surface area, high κ, and impressive electrical conductivity [8, 9]. Graphene is widely used as a photocatalyst and in TE applications because it has superior electron transport abilities. In Japan, Mitsui Mining & Smelting has developed a TE generator using rGO-doped bismuth titanate to convert waste heat into energy, currently undergoing industrial testing [10, 11]. Affordable low-temperature TE materials like rGO-doped bismuth titanate and silver telluride composites hold promise for transforming energy generation by converting heat to electricity even at lower temperatures. These TE composites are produced using environmentally friendly and cost-effective hydrothermal synthesis methods, contrasting with traditional, expensive, and hazardous techniques [11].

2. Literature Review

Numerous strategies have been proposed for the economical and environmentally friendly synthesis of TE materials. These include utilizing natural and sustainable resources like plant extracts, biomaterials, and agricultural waste [10, 11]. Such resources are abundant, renewable, and cost-effective [9–11]. Designing synthesis routes that minimize waste, reduce energy consumption, and ensure safety for both humans and the environment is crucial. Techniques such as the Sol-Gel Method and Wet Chemical Methods (e.g., co-precipitation, chemical reduction, or electrochemical deposition) offer scalable and cost-effective production of high-quality TE materials.

Furthermore, using recyclable templates made from biodegradable materials aids in structuring TE materials while diminishing waste and environmental impact during synthesis. Conducting a life cycle analysis is essential for a comprehensive evaluation of the environmental impact throughout the synthesis process, pinpointing areas for improvement [12, 13]. Researchers have also developed TE materials incorporating n-type bismuth titanate (BTO)-doped rGO, akin to Ag_2Te-doped rGO [12, 13]. The combination of rGO and BTO forms a heterojunction at the interface of the materials. This junction acts as a barrier to the movement of holes while allowing the flow of electrons, thus boosting the electrical conductivity of the composite without compromising the Seebeck coefficient [13, 14]. The extensive surface area of rGO offers numerous locations for BTO nanostructure growth, leading to a nanocomposite with a high density of grain boundaries and further enhancing its TE properties.

The novelty of this research paper delves into using an rGO-doped silver telluride composite as a p-type TE. In this research work, we report novel TE characteristics of rGO-doped (5%, 10%, and 15% in vol for both films) BTO (N-type) and Ag_2Te(P-type) through low-cost sol-gel synthesis methods. A new TE material was created with more significant Seebeck coefficients, reduced thermal conductivities, and improved efficiency at low temperatures. Including RGO contributes to a high Seebeck coefficient, as it facilitates efficient charge carrier transport and enhances the density of states near the Fermi level. The integration of RGO imparts superior mechanical strength and flexibility to the nanocomposites, making them more robust and durable under thermal cycling conditions. The synthesized novel materials exhibit excellent thermal stability, attributed to the inherent stability of oxide materials and the reinforcing effect of rGO, which prevents degradation at high temperatures. Our method's precursor materials and solvents are readily available and inexpensive. This makes the synthesis process more economical than methods requiring rare or costly elements. This research paper also reflects the use of low-cost reducing agents to fabricate novel TE p- and n-side junctions. Traditional synthesis methods often involve toxic solvents, high energy consumption, and expensive raw materials [14–16].

In contrast, our approach incorporates several key benefits. We utilized ethylene glycol-based graphene as a reducing agent, which is less toxic and more biodegradable compared to conventional reducing agents like hydrazine or sodium borohydride [16–18]. This reduces the environmental impact of the synthesis process. The sol-gel method employed in our study operates at relatively low temperatures and shorter reaction times than traditional high-temperature solid-state reactions. This leads to significant energy savings and a reduced carbon footprint. Our process generates minimal byproducts and waste, as the precursor materials are efficiently converted into the desired TE composites [18–22]. This contrasts with traditional methods that often produce large amounts of hazardous waste. Our method can be integrated into existing manufacturing facilities with minimal modifications. This compatibility reduces the need for substantial capital investment in new infrastructure.

In this research, our objectives are as follows:

- A TE energy conversion device utilizes fabricated multifunctional nanocomposite films containing rGO-doped Ag_2Te and BTO.
- Including rGO reduces the double Schottky barrier, thereby improving electrical conductivity and the ZT.
- The nanocomposite was tailored to improve TE properties by carefully shaping nanomaterial morphology.

3. Research Method

This study employed a comprehensive approach to investigate TE materials, combining experimental synthesis, structural characterization, and performance evaluation. The synthesis involved precise control of precursor ratios and doping, followed by advanced techniques such as X-ray diffraction (XRD) and field emission scanning electron microscopy (FESEM) for detailed structural and morphological properties analysis. Figure 1 shows the schematic presentation of our research.

3.1. Materials

The dopant precursor material was graphene oxide powders (GO) with a 99% purity, obtained from Sigma-Aldrich. The electrolyte precursor for the tellurium nanowire was created by dissolving tellurium dioxide (TeO_2) from Alfa Aesar, Inc. (99.995% purity) in ethylene glycol (Sigma-Aldrich, 99.8% purity) and then adding hydroxylamine silver telluride (Ag_2Te) materials were synthesized by reacting tellurium nanowires with silver nitrate ($AgNO_3$; ACS reagent, 99.0% purity, Sigma-Aldrich). Additionally, BTO was prepared using a sol-gel process involving bismuth nitrate pentahydrate ($Bi(NO_3)_3{\cdot}5H_2O$) and titanium tetra-isopropoxide ($Ti(OiPr)_4$), both with 99.0% purity and sourced from Sigma-Aldrich [23, 24].

3.2. Synthesis of rGO

We prepared various rGO samples with different levels of oxygen groups (high, mild, and low) by reducing GO using

Figure 1
Schematic presentation of the mechanism of the Seebeck effect in thermoelectricity

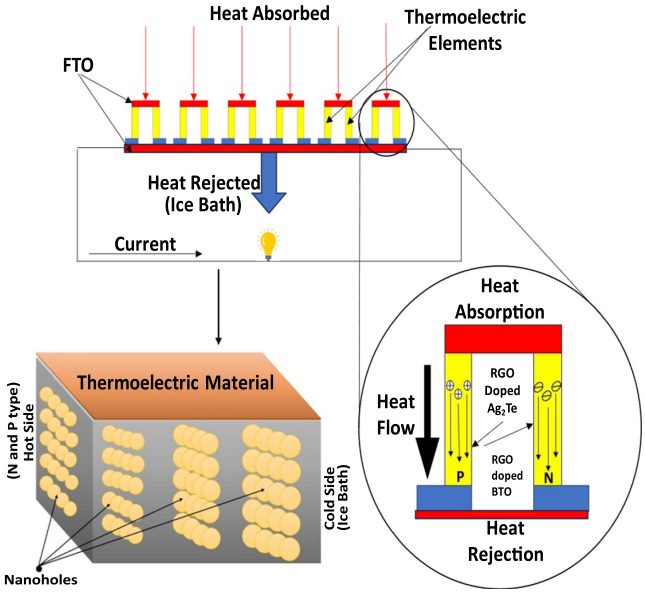

different concentrations of hydrazine (0.1%, 0.15%, and 0.5% by weight) and varying reduction times (5, 10, 15 min). These rGO samples were then added to mortar composites at an optimal dosage of 0.1%. Characterization methods such as FESEM and XRD were employed to study these samples. The inclusion of 0.1% rGO, produced through a 15-minute reduction process using 0.2% hydrazine and containing moderate oxygen groups, resulted in a notable performance increase compared to composites made with GO. More specifically, there was a maximum improvement of 44.0% and 83.7% in certain properties, surpassing the results obtained with GO (37.5% and 77.7%, respectively). These findings emphasize the significant influence of oxygen groups and the crystallinity of graphene structures on the physical, chemical, and mechanical properties. The intricate relationship between these factors underscores the importance of achieving a delicate balance to attain an optimal level of oxygen groups on rGO sheets for effective bonding between them [14–16].

3.3. Synthesis of rGO-doped silver telluride nanostructures

A simple wet chemical approach created a rGO-doped silver telluride nanostructure. rGO was dispersed in distilled water and sonicated to create a uniform dispersion. Separate solutions of $AgNO_3$ and TeO_2 were prepared similarly. The rGO dispersion was mixed with the $AgNO_3$ and TeO_2 solutions while stirring. These doped composite films were deposited on fluorine-doped tin oxide (FTO) substrates as P-type films by spin coating onto FTO glass [25, 26].

3.4. Synthesis of rGO-doped bismuth titanate nanostructures

To dope rGO with BTO, a solution of bismuth nitrate ($Bi(NO_3)_3$) and titanium tetra-isopropoxide ($Ti(O\text{-}i\text{-}Pr)_4$) in isopropanol is added to the rGO suspension. The mixture is then sonicated for 30 min before refluxing at 80°C for 2 h. The resultant residue is washed and filtered to remove contaminants. The resultant residue is washed and filtered to remove contaminants. We used ethylene glycol as a solvent here [27–29]. Ethylene glycol is a solvent with a high boiling point that prevents BTO nanostructure aggregation. The Sol-gel synthesis approach creates an rGO-doped BTO nanostructure with homogeneous size and shape. We deposited this film as N-type on the FTO substrate by spin coating.

4. Fabrication and Measurement of TE Device

The attached N-type and P-type films (labeled as A and B) were deposited on FTO using cold and hot surface connections. As illustrated in Figure 1, our TE generator setup featured cold and hot surfaces positioned at the ends of a thermocouple. The system's κ and Seebeck coefficient were measured using a current source. Our setup involved a TE generator with distinct cold and hot surfaces positioned at the ends of a thermocouple to create the necessary temperature gradient for TE operation. This gradient facilitated the diffusion of charge carriers from the hot to the cold side, generating a voltage through the Seebeck effect. Detailed measurements and analyses of the N-type and P-type films allowed for the assessment of their contributions to the overall performance of the TE generator. Through precise control and characterization of these parameters, we aimed to optimize the efficiency and effectiveness of our TE system.

L represents the distance, R represents the resistance, Ta and Tb are the temperature of the electrodes, and A is the ammeter used to measure the flowing current. A current source was employed in the experimental setup to measure the κ of the films accurately. The κ data, combined with the temperature differential across the thermocouple, allowed us to calculate the Seebeck coefficient of the system. This coefficient is critical for evaluating the efficiency of the TE materials, as it measures the magnitude of the voltage generated per unit temperature difference across the material as shown in Figure 2.

Figure 2
Schematic presentation of thermoelectric generator (TEG) made of N- and P-type rGO-doped Ag_2Te and BTO composite, respectively

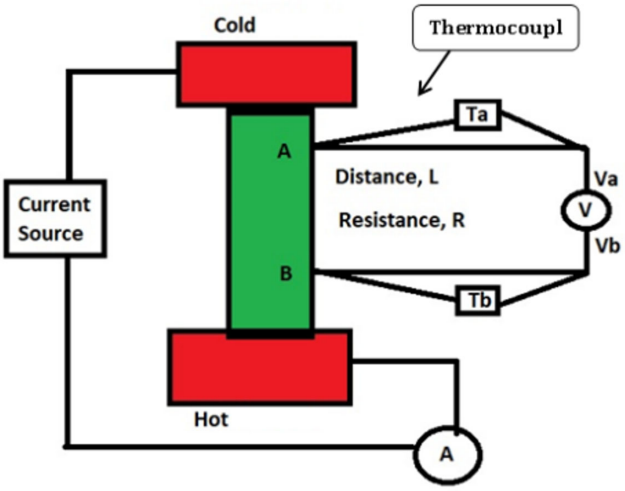

5. Experimental Section

Morphological analysis was performed using XRD and FESEM. TE parameters were measured using a Keithley 2450 Electrometer. Phase formation was identified using powder XRD

Figure 3
The experimental setup includes the fabrication of thermoelectric materials, the annealing process, the experimental observations, and the outcome

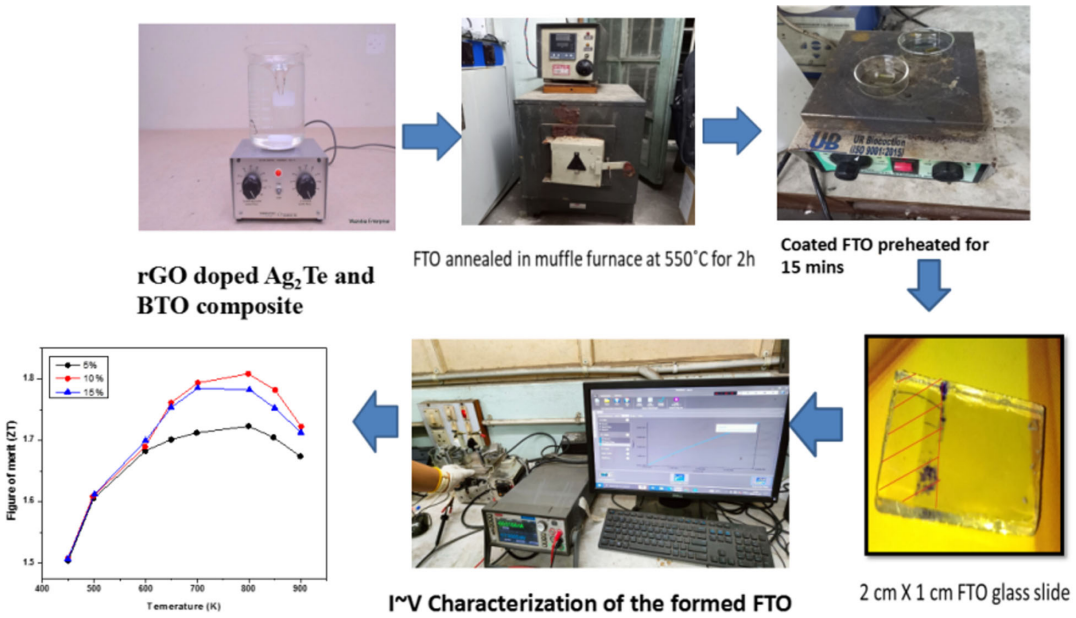

with Cu Kα radiation [29]. The Keithley 2450 source meter instrument was employed to measure both electrical conductivity and the Seebeck coefficient at the same time [30]. The product of the thermal diffusivity, heat capacity, and experimental density determined the κ at ambient temperature. The experimental arrangement of the TE device is depicted in Figure 3.

5.1. Scanning electron microscopy

FESEM (JEOL JSM-7600F) was performed to determine the morphology, which is essential in thin film photovoltaic and morphological performance [31, 32]. Figure 2 shows the morphology of the (a) 10% rGO-doped BTO and (b) 10% RGO-doped Ag_2Te TE materials on a 100-nanometer scale. The surface characteristics of the prepared samples, as evidenced by the FESEM images in Figures 3(a)-(b), exhibited BTO uniform nanostructures. However, the 10% (Vol) rGO composite images reveal agglomerated nanorods coexisting with sheet-like rGO structures, as depicted in Figure 4. Figure 4(a) portrays the rod-like porous structures of approximately 25 nm particle size. Figure 4(b) portrays the doped p-type composite with porous and uniform distribution.

Figure 4
FESEM images of thin film(a) 10% rGO-doped BTO n-side nanocomposite (b) 10% doped rGO p-side Ag_2Te composite

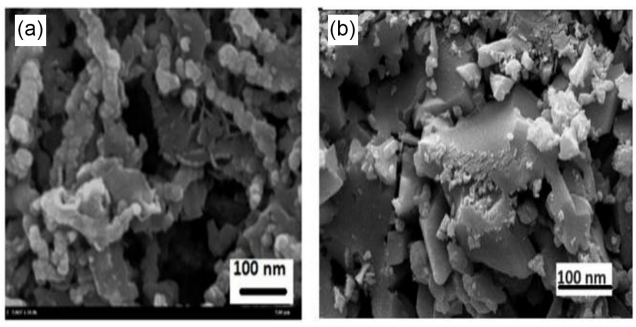

5.2. XRD

The phase analysis of the synthesized rGO-doped BTO was performed using XRD with a Miniflex-ZD06184 (Rigaku) instrument, featuring a graphite monochromator and Cu Kα radiation (λ = 1.54 Å) operating at 40 kV and 30 mA at room temperature (refer to Figure 3). All diffraction peaks of the initial mixture were indexed to the bismite structure of Bi_2O_3. Due to this, all peaks appeared to be significantly broad, indicating a decrease in crystallite size. Notably, in the BTO-rGO composite with a 10% rGO concentration, the XRD peaks do not show any characteristic diffraction peaks of GO. This absence can be attributed to the low concentration of graphene, its weak diffraction intensity, and the disrupted stacking caused by the intercalation of BTO particles. Bismuth and titanium ions act as donors in these systems, and their interactions with the conduction band are minimal, as confirmed by band calculations [17]. Furthermore, incorporating $Bi_4Ti_3O_{12}$ particles onto rGO sheets does not alter their phase [30, 31]. Figure 3 inset shows that $Bi_4Ti_3O_{12}$ crystallizes in the orthorhombic Aea2 space group, with a structure similar to $Pb(Zr_{0.50}T_{i0.48})O_3$. There are two distinct Ti^{4+} sites. The first Ti^{4+} site is bonded to six O^{2-} atoms in a 6-coordinate geometry, with Ti-O bond distances ranging from 1.77 to 2.32 Å. In the second Ti^{4+} site, Ti^{4+} bonds with six O^{2-} atoms to form corner-sharing TiO_6 octahedra, with corner-sharing octahedral tilt angles of 20° and Ti-O bond distances ranging from 1.85 to 2.06 Å. There are also two distinct Bi^{3+} sites. In the first Bi^{3+} site, Bi^{3+} is bound in a 6-coordinate geometry to six O^{2-} atoms, with Bi-O bond distances ranging from 2.20 to 2.53 Å [28–31]. The third O^{2-} site has a distorted see-saw-like geometry with two Ti^{4+} and two equivalent Bi^{3+} atoms. The fourth O^{2-} site is bound in a 2-coordinate geometry to two Ti^{4+} and one Bi^{3+} atom. The fifth O^{2-} site bonds with four equivalent Bi^{3+} atoms, forming a mix of edge and corner-sharing OBi_4 tetrahedra. In the sixth O^{2-} site, O^{2-} is bound in a 3-coordinate geometry to two equivalent Ti^{4+} and one Bi^{3+} atom.

Figure 4(b) illustrates the crystallinity analysis and purity of the synthesized material. The pattern exhibits a distinct peak centered at 25.2 degrees, corresponding to the (0, 0, 2) Miller indices. This peak

indicates the presence of the 10% rGO-doped BTO crystal plane, which showed the best XRD characterization among the three doped composites. Figure 4 illustrates the density of states and the average absorption effect of bismuth, tellurium, and oxygen content. Alloys with a line-ordered structure have a smaller band gap than those with a random and clustered composite distribution, as determined through structural XRD analysis [32, 33]. The optimal plot is obtained for the 10% doped sample, showing the highest peak at Miller indices (0, 0, 2). The peak for the 5% doped nanocomposite was observed around (2, 1, 0), and for the 15% doped sample, the highest peak was found at (1, 1, 7) according to literature data [33, 34]. The lattice parameters of the compound decreased along the a- and c-axes with an increase in oxygen concentration. However, when RGO was doped into the material, the lattice parameters along the a- and c-axes increased slightly. This change is likely due to GO atoms occupying the van der Waals gaps and iodine substituting at Ti vacancy sites. Generally, XRD peak broadening can be attributed to crystal domain size and micro-strain. The Williamson–Hall relation represents lattice strain and grain size using lower-resolution XRD data from peak positions and widths, as given by Equation (2) [34–36]:

$$\beta cos(\theta) = \mathrm{rK}\lambda + 4\sigma \sin(\theta) \quad (2)$$

In the given information:

- The parameter β represents the peak's full width at half maximum.
- The symbol θ denotes the Bragg angle.
- The term (r) stands for the size of the crystalline domain.
- The character σ is used to indicate micro-strain fluctuation.
- The symbol λ represents the incident X-ray wavelength.
- K is a dimensionless shape factor, usually around 0.9.

Non-uniform lattice distortion, dislocations, anti-phase domain boundaries, and grain surface relaxation can cause micro-strain.

6. Results and Discussions

The following sections summarize the results of the studies that were assessed:

N and P doping: We opted for commercially available dopant rGO to incorporate into the p- and n-side nanomaterials to explore the electrical characteristics. This choice was made due to its robust n-doping capability, exceptional chemical stability, and ease of solution processing. Following thermal annealing at 120°C for 4 hours, the conductivity was assessed using the two-point or four-point probe method.

6.1. Electrical conductivity and Seebeck coefficient

The electrical conductivity and Seebeck coefficient of both doped materials consistently increase with the temperature in Figures 6(a)-(c). This behavior is explained by the effective promotion of charge carriers from the valence band to the conduction band by thermal energy, making them readily available for electrical conduction [35, 36]. It is worth noting that the electrical conductivity of rGO-doped bismuth titanate outperforms that of rGO-doped silver telluride across all temperature ranges due to the higher electron mobility of bismuth titanate. The κ decreases consistently with increasing temperature, primarily influenced by lattice contributions [27, 35]. This solid solution is anticipated to exhibit a significant reduction in κ, highlighting the potential for improved TE properties, as shown in Figure 5.

Figure 5
X-ray diffraction analysis of 5%, 10%, and 15% rGO-doped nanocomposite thin film

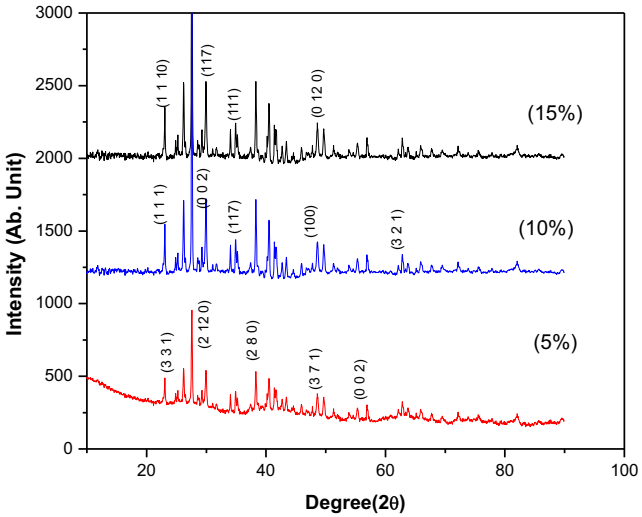

To better understand the adding rGO and its influences on the properties, we utilized the Pisarenko relation to analyze the relationship between S and NH [33, 34]. By applying a model based on a single parabolic band and assuming energy-independent carrier scattering in degenerate semiconductors, we derived the following Equation (3):

$$S = 8\pi^2 k^2 Tm * /3eh^2(\pi/3n)^{2/3} \quad (3)$$

Here, k, e, h, and n represent the Boltzmann constant, electronic charge, Planck constant, and carrier concentration, respectively. The 10% doped nanocomposite exhibited the best Seebeck coefficient and electrical conductivity.

6.2. Thermal conductivity

Figure 6 depicts the temperature-dependent behavior of κ. κ decreases with increasing temperature across the range, indicating that lattice contributions dominate as per the literature [27]. This outcome can be attributed to variations in atomic bond strength, with scattering from grain boundaries and carriers showing comparable effects. It seems that changes in the strength of bonds have a bigger impact on κ compared to the spread of point defects [28] within this specific system. κ in this scenario consists of two separate elements: the lattice component and the electronic component. The transfer of heat and electrical charge is carried out by charge carriers, which are electrons in n-type semiconductors and holes in p-type semiconductors. The Wiedemann-Franz law describes the κ of electronic components as κe = LσT. The Lorenz number (L) is a key factor in this equation, and it ranges from 1.44 to 2.44 108 WK^2 for non-degenerate electron gas to fully degenerated electron gas, respectively. The literature review found that the value of the very degraded number (L = 2.44 108 WK^2) [29] results in an underestimate of the lattice κ, which can reach 40%. It is highest for the 0.10 molar ratio of the doped composite. Thermal conductivity vs temperature has been shown in Figure 7. It shows the best optimal curve for 10% doped composite.

6.3. Figure of merit

The merit Figure for TE materials can be seen in Figure 8(a), which illustrates the ZT derived from the above data. It was

Figure 6
(a) Graphs depicting the relationship between electrical conductivity and Seebeck coefficient with temperature for 5% doped rGO-BTO (N-type) and Ag_2Te (P-type) composites, (b) 10% doped rGO-BTO (N-type) and Ag_2Te (P-type) composites, and (c) 15% doped rGO-BTO (N-type) and Ag_2Te (P-type) composites

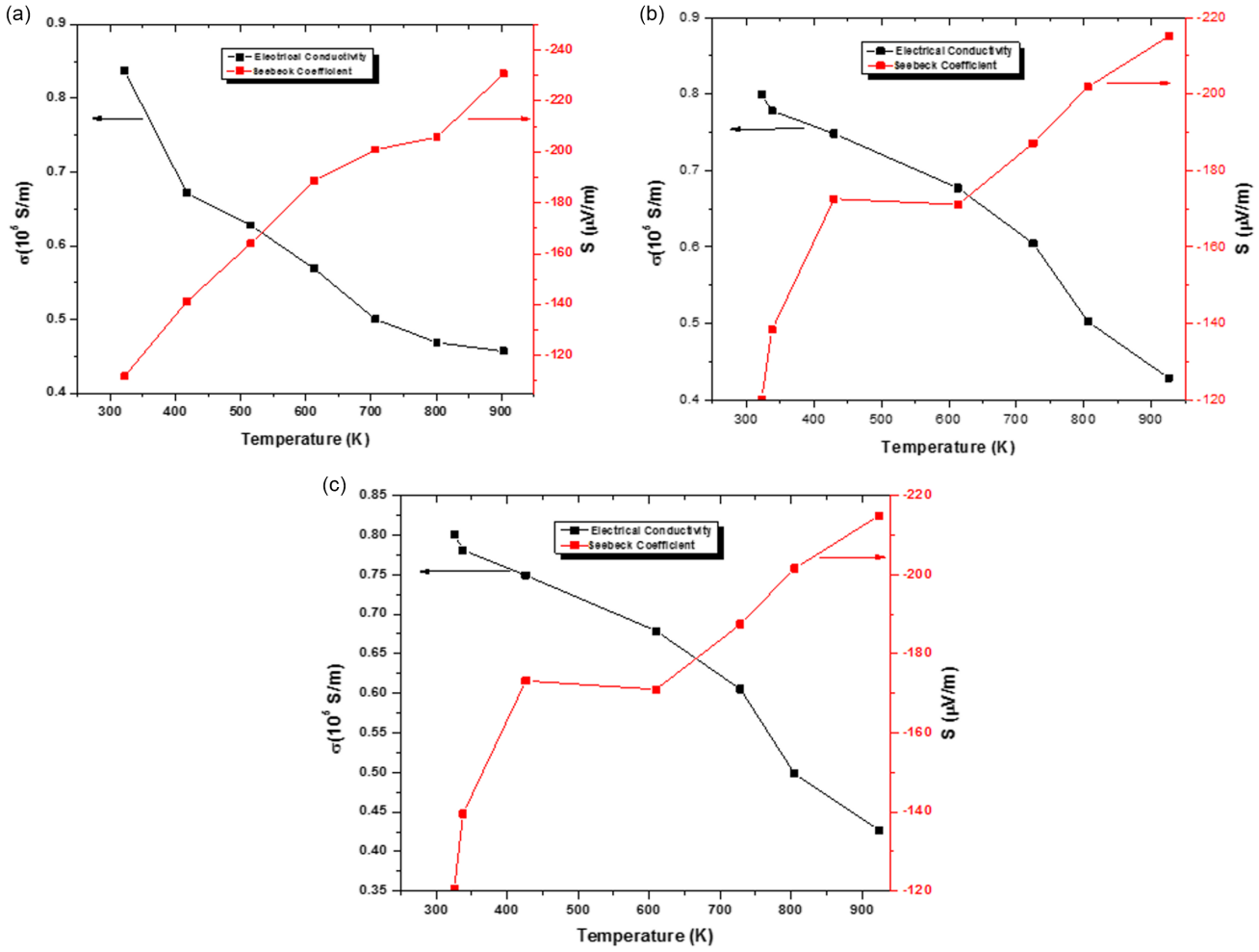

Figure 7
Thermal conductivity vs temperature for 5%, 10%, and 15% rGO-doped BTO(N-type) and rGO-doped Ag_2Te(P-type) thin film composite

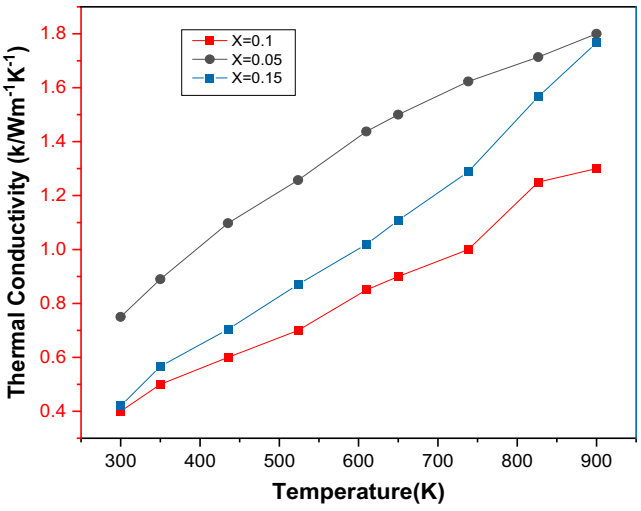

identified that the ZT is optimized for a 1:10 molar ratio at 750 K, yielding a value of 1.78*104 K^{-1}. It is worth noting that BTO-doped rGO and Ag2Te-doped rGO exhibit a slightly higher ZT, attributed to a more significant decrease in κ. As the lattice parameter impacts electrical properties, a shorter Ti-Ti distance is preferable for enhancing the PF. To further improve the ZT, efforts should focus on concurrently reducing heat conductivity, adjusting the Ti-Ti distance, and maintaining the cubic ratio constant. As the temperature increases, the TE ZT initially rises and then declines after 330 K. This pattern is due to the enhanced electrical conductivity that occurs with rising temperatures. At higher temperatures, peak ZT values are achieved for rGO-doped BTO (N-type) and rGO-doped Ag_2Te (P-type) thin film composites. This is largely because the Seebeck coefficient remains relatively stable at elevated temperatures. Notably, the peak ZT for rGO-doped BTO typically exceeds the maximum ZT for rGO-doped Ag_2Te. This difference can be attributed to the inherently higher Seebeck coefficient of BTO than Ag_2Te.

Furthermore, Figure 8(b) shows the link between power-generating efficiency and average ZT_{ave} from Equation (4) [29, 30]:

Figure 8
(a) Figure of merit vs. temperature for 5%, 10%, and 15% rGO-doped BTO(N-type) and rGO-doped Ag_2Te(P-type) composites, (b) experimental conversion efficiency as a function of temperature gradient for the doped nanocomposite sample, along with the figure of merit

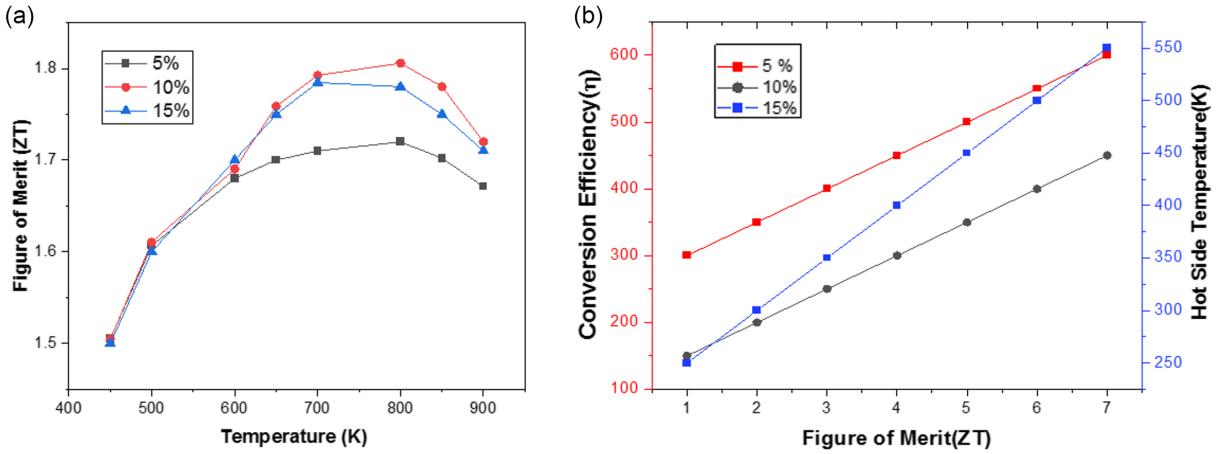

Figure 9
Power factor of 5%, 10%, and 15% rGO-doped BTO(N-type) and rGO-doped Ag_2Te(P-type) composites

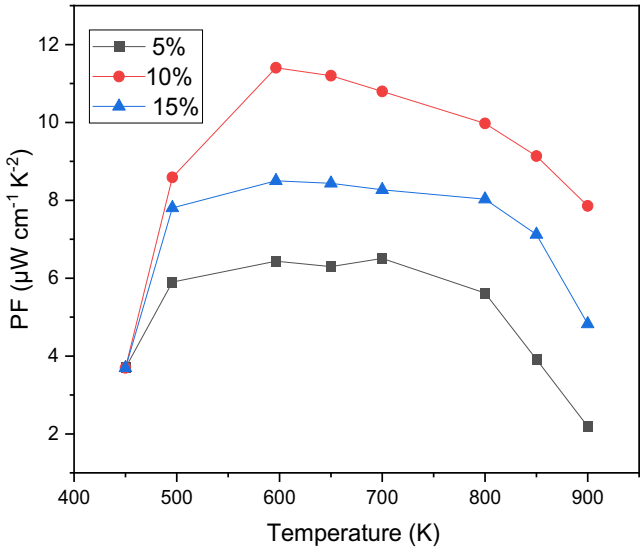

$$\eta p = \frac{Th - Tc}{Th}(((\sqrt{(1 + ZTave)} + 1)/(\sqrt{(1 + \mathrm{ZTave})} + \mathrm{Tc/Th})) \quad (4)$$

ZT_{ave} represents the average value of both n-type and p-type legs, calculated across the temperature-dependent ZT curve between Th and Tc, where Th and Tc denote the temperatures at the hot and cold ends, respectively [30]. The illustration highlights that a higher ZTave and a broader temperature differential increase conversion efficiency. For instance, at ZTave = 4.0 and ΔT = 500 K, the power generation efficiency (ηp) can achieve 25%, comparable to traditional heat engines, using a 10 percent doped composite [30–34]. The Seebeck effect is fundamental for generating TE power, proving essential in certain extreme scenarios or exceptional circumstances. Radioisotope TE generators (RTGs) have a longstanding history of powering satellites and space probes like Apollo 12, Voyager 1, and Voyager 2. TE power generation is gaining traction in advanced scientific fields, with thermal sources ranging from fuels, waste heat, geothermal energy, and solar energy to radioisotopes [33, 34].

6.4. Power factor

The performance of TE materials is characterized by $PF = S^2\sigma$, which is one of the main parameters. The PF of the rGO nanocomposites increased significantly with increasing pressure. During the first pressurization cycle, it achieved PF values of 10^{-12} W cm^1K^2 at approximately 5 GPa, and during subsequent cycles, it reached PF values of 8^{-10} W $cm^{-1}K^{-2}$ as shown in Figure 9, as shown in Figure 8. Band-gap tuning is recognized as a beneficial strategy for optimizing the PF of a semiconductor TE, as electrical resistivity and the band gap influence thermopower in distinct manners [34, 37].

7. Conclusions

A new set of stable TE materials was synthesized through chemical synthesis using elements abundant in the earth and environmentally friendly. Polycrystalline rGO-doped BTO (N-type) and Ag_2Te (P-type) thin films were synthesized via a solid-state process and deposited by spin coating technique. Our report highlights the electrical conductivity, the Seebeck coefficient, and κ of our fabricated TE composites at temperatures ranging from ambient temperature to 500 K. We observed the Seebeck coefficient, electrical conductivity increased, and decreased κ with temperature increase. We also observed unexpectedly, as RGO concentrations grew, κ increased, contradicting the predictions of point defect scattering theory. Around 873 K, BTO/rGO composites have a ZT of up to $1.8*10^{-4}$ K^{-1}, more significant than the average Ag_2Te-rGO composites and higher than the ZT of undoped silver telluride.

Additionally, our discovery has led to the development of new N-type and P-type TE materials with higher TE ZT. The TE properties of these materials are enhanced by doping with RGO. This finding has also reduced the cost and complexity of

fabricating TE devices. It is important to note that although research in this area is ongoing and shows promise, the practical application of rGO-doped BTO and Ag_2Te TE materials is still in the developmental stage. This research is focused on optimizing these materials to meet the efficiency and reliability standards required for commercial and widespread use, aiming to achieve better ZT at room temperature. The potential scalability of our synthesis process for industrial applications is promising. The sol-gel method allows for modular scaling, where production capacity can be increased by adding more reaction modules without significant changes to the process. This modularity is advantageous for gradually scaling up production to meet market demand. In conclusion, our environmentally friendly and cost-effective synthesis methods offer significant advantages over traditional methods. The scalability of the sol-gel process and the use of green solvents and materials position our approach as a viable solution for industrial applications in the TE materials market.

Acknowledgement

The author (S. Roy) would like to acknowledge "Scheme for Transformational and Advanced Research in Sciences (STARS)" (MoE-STARS/STARS-2/2023-0175) by the Ministry of Education for promoting translational India-centric research in sciences implemented and managed by Indian Institute of Science (IISc), Bangalore, for their support.

Ethical Statement

This study does not contain any studies with human or animal subjects performed by any of the authors.

Conflicts of Interest

The authors declare that they have no conflicts of interest to this work.

Data Availability Statement

Data are available from the corresponding author upon reasonable request.

Author Contribution Statement

Jyoti Bhattacharjee: Conceptualization, Methodology, Software, Validation, Formal analysis, Investigation, Resources, Data curation, Writing – original draft, Writing – review & editing. **Subhasis Roy:** Conceptualization, Methodology, Software, Validation, Formal analysis, Investigation, Resources, Data curation, Writing – original draft, Writing – review & editing, Visualization, Supervision, Project administration.

References

[1] Acharya, M., Jana, S. S., Ranjan, M., & Maiti, T. (2021). High-performance (ZT>1) n-type oxide thermoelectric composites from earth-abundant materials. *Nano Energy*, *84*, 105905. https://doi.org/10.1016/j.nanoen.2021.105905

[2] Ashfaq, A., Almufarij, R. S., Shokralla, E. A., Alharbe, L. G., Alqurashi, H., Rehman, U., & Somaily, H. H. (2024). Enhanced thermoelectric properties and thermal stability of $Cu_{1.8}S$-rGO nanocomposite by low energy carrier filtering effect. *Diamond and Related Materials*, *144*, 111037. https://doi.org/10.1016/j.diamond.2024.111037

[3] Bantawal, H., Shenoy, U. S., & Bhat, D. K. (2018). Tuning the photocatalytic activity of $SrTiO_3$ by varying the Sr/Ti ratio: Unusual effect of viscosity of the synthesis medium. *The Journal of Physical Chemistry C*, *122*(34), 20027–20033. https://doi.org/10.1021/acs.jpcc.8b06514

[4] Bhattacharjee, J., & Roy, S. (2024). A review on photocatalysis and nanocatalysts for advanced organic synthesis. *Hybrid Advances*, *6*, 100268. https://doi.org/10.1016/j.hybadv.2024.100268

[5] Burriel, M., Wilkins, S., Hill, J. P., Muñoz-Márquez, M. A., Brongersma, H. H., Kilner, J. A., …, & Skinner, S. J. (2014). Absence of Ni on the outer surface of Sr doped La_2NiO_4 single crystals. *Energy & Environmental Science*, *7*(1), 311–316. https://doi.org/10.1039/C3EE41622D

[6] Choi, G., Kim, H. S., Lee, K., Park, S. H., Cha, J., Chung, I., & Lee, W. B. (2017). Study on thermal conductivity and electrical resistivity of Al-Cu alloys obtained by Boltzmann transport equation and first-principles simulation: Semi-empirical approach. *Journal of Alloys and Compounds*, *727*, 1237–1242. https://doi.org/10.1016/j.jallcom.2017.08.156

[7] Bhattacharjee, J., & Roy, S. (2024). Significance of renewable energy in water management and irrigation. In S. Suriyanarayanan, H. P. Shivaraju, & D. Jenkins (Eds.), *Water management in developing countries and sustainable development*, (pp. 235–252). Springer. https://doi.org/10.1007/978-981-99-8639-2_12

[8] Celebi, N., Arlı, F., Soysal, F., & Salimi, K. (2021). Z-scheme ZnO@ PDA/CeO_2 heterojunctions using polydopamine as electron transfer layer for enhanced photoelectrochemical H_2 generation. *Materials Today Energy*, *21*, 100765. https://doi.org/10.1016/j.mtener.2021.100765

[9] Cho, H., Back, S. Y., Kim, J. H., Inturu, O., Lee, H. S., & Rhyee, J.-S. (2019). Enhancement of thermoelectric properties over a wide temperature range by lattice disorder and chemical potential tuning in a $(CuI)_y(Bi_2Te_3)_{0.95-x}(Bi_2Se_3)_x(Bi_2S_3)_{0.05}$ quaternary system. *RSC Advances*, *9*(8), 4190–4197. https://doi.org/10.1039/c8ra09280j

[10] Druce, J., Téllez, H., Burriel, M., Sharp, M. D., Fawcett, L. J., Cook, S. N., …, & Kilner, J. A. (2014). Surface termination and subsurface restructuring of perovskite-based solid oxide electrode materials. *Energy & Environmental Science*, *7*(11), 3593–3599. https://doi.org/10.1039/C4EE01497A

[11] Du, Y., Li, J., Xu, J., & Eklund, P. (2019). Thermoelectric properties of reduced graphene oxide/Bi_2Te_3 nanocomposites. *Energies, 12*(12), 2430. https://doi.org/10.3390/en12122430

[12] Gautam, A. K., & Khare, N. (2023). Enhanced thermoelectric figure of merit at near room temperature in n-type binary silver telluride nanoparticles. *Journal of Materiomics*, *9*(2), 310–317. https://doi.org/10.1016/j.jmat.2022.10.003

[13] Hatzikraniotis, E., Polymeris, G. S., & Kyratsi, T. (2024). Thermal conductivity in thermoelectric materials. In R. Vargas-Bernal & R. Palma Guerrero (Eds.), *Novel applications of piezoelectric and thermoelectric materials* (pp. 83–102). IntechOpen. https://doi.org/10.5772/intechopen.106168

[14] He, Y., Day, T., Zhang, T., Liu, H., Shi, X., Chen, L., & Snyder, G. J. (2014). High thermoelectric performance in non-toxic earth-abundant copper sulfide. *Advanced Materials 26*(23), 3974–3978. https://doi.org/10.1002/adma.201400515

[15] Holmström, E., & Foster, A. S. (2017). Adsorption of water onto $SrTiO_3$ from periodic Møller-Plesset second-order perturbation theory. *Journal of Chemical Theory and Computation*, *13*(12), 6301–6307. https://doi.org/10.1021/acs.jctc.7b00549

[16] Holmström, E., Spijker, P., & Foster, A. S. (2016). The interface of $SrTiO_3$ and H_2O from density functional theory molecular dynamics. *Proceedings of the Royal Society A: Mathematical, Physical and Engineering Sciences*, *472*(2193). https://doi.10.1098/rspa.2016.0293

[17] Barbaros, I., Yang, Y., Safaei, B., Yang, Z., Qin, Z., & Asmael, M. (2022). State-of-the-art review of fabrication, application, and mechanical properties of functionally graded porous nanocomposite materials. *Nanotechnology Reviews*, *11*(1), 321–371. https://doi.org/10.1515/ntrev-2022-0017

[18] Islam, A. N. M. F., Islam, R., Javed, S., & Saha, S. (2024). Optimization of system parameters during conjugate mixed convective flow in a square domain with an oscillating spinning cylinder. *Heliyon*, *10*(2), e24258. https://doi.org/10.1016/j.heliyon.2024.e24258

[19] Ji, J. H., Lee, G., & Koh, J. H. (2022). Synthesis of a nitrogen-doped reduced graphene oxide-based ceramic polymer composite nanofiber film for wearable device applications. *Scientific Reports*, *12*(1), 15583. https://doi.org/10.1038/s41598-022-19234-0

[20] Jasim, O. M. J., Selimli, S., Dumrul, H., & Yilmaz, S. (2022). Closed-loop aluminum oxide nanofluid cooled photovoltaic thermal collector energy and exergy analysis, an experimental study. *Journal of Energy Storage*, *50*, 104654. https://doi.org/10.1016/j.est.2022.104654

[21] Khoso, N. A., Jiao, X., GuangYu, X., Tian, S., & Wang, J. (2021). Enhanced thermoelectric performance of graphene-based nanocomposite coated self-powered wearable e-textiles for energy harvesting from human body heat. *RSC Advances, 11*(27), 16675–16687. https://doi.org/10.1039/d0ra10783b

[22] Kumuda, S., Gandhi, U., Mangalanathan, U., & Rajanna, K. (2024). Synthesis and characterization of graphene oxide and reduced graphene oxide chemically reduced at different time duration. *Journal of Materials Science: Materials in Electronics*, *35*(9), 637. https://doi.org/10.1007/s10854-024-12393-y

[23] Lazarevic, Z. Z., Romcevic, N. Z., Todorovic, M., & Stojanovic, B. D. (2007). Structural and ferroelectrical properties of bismuth titanate ceramic powders prepared by mechanically assisted synthesis. *Science of Sintering*, *39*(2), 177–184. https://doi.org/10.2298/sos07021771

[24] Liu, X., Li, S., Yu, J., Zhu, Y., Lin, K, Wang, B., & Freer, R. (2024). Enhancing the thermoelectric properties of TiO_2-based ceramics through addition of carbon black and graphene oxide. *Carbon*, *216*, 118509. https://doi.org/10.1016/j.carbon.2023.118509

[25] Okhay, O., & Tkach, A. (2021). Impact of graphene or reduced graphene oxide on performance of thermoelectric composites. *C*, *7*(2), 37. https://doi.org/10.3390/c7020037

[26] Pazarlıoğlu, H. K., Gürsoy, E., Gürdal, M., Tekir, M., Gedik, E., Arslan, K., & Taşkesen, E. (2023). The first and second law analyses of thermodynamics for $CoFe_2O_4/H_2O$ flow in a sudden expansion tube inserted elliptical dimpled fins. *International Journal of Mechanical Sciences*, *246*, 108144. https://doi.org/10.1016/j.ijmecsci.2023.108144

[27] Reshma, R. P., Abishek, N. S., & Gopalakrishna, K. N. (2024). Synthesis and characterization of graphene oxide, tin oxide, and reduced graphene oxide-tin oxide nanocomposites. *Inorganic Chemistry Communications*, *165*, 112451. https://doi.org/10.1016/j.inoche.2024.112451

[28] Shaikh, A. A., Bhattacharjee, J., Datta, P., & Roy, S. (2024). A comprehensive review of the oxidation states of molybdenum oxides and their diverse applications. *Sustainable Chemistry for the Environment*, *7*, 100125. https://doi.org/10.1016/j.scenv.2024.100125

[29] Kim, S., Ryu, S. H., Kwon, Y.-T., Lim, H.-R., Park, K.-R., Song, Y., & Choa, Y.-H. (2017). Synthesis and thermoelectric characterization of high-density Ag_2Te nanowire/PMMA nanocomposites. *Materials Chemistry and Physics*, *190*, 187–193. https://doi.org/10.1016/j.matchemphys.2017.01.019

[30] Shen, H., Jang, B., Park, J., Mun, H.-J., Cho, H.-B., & Choa, Y.-H. (2022). In Situ synthesis of a Bi_2Te_3-nanosheet/reduced-graphene-oxide nanocomposite for non-enzymatic electrochemical dopamine sensing. *Nanomaterials*, *12*(12), 2009. https://doi.org/10.3390/nano12122009

[31] Shah, S. A. A., Idrees, M., Bariq, A., Ahmad, B., Ali, B., Ragab, A. E., & Az-Zo'bi, E. A. (2024). Comparative study of some non-Newtonian nanofluid models across stretching sheet: A case of linear radiation and activation energy effects. *Scientific Reports*, *14*(1), 4950. https://doi.org/10.1038/s41598-024-54398-x

[32] Snyder, G. J., & Toberer, E. S. (2008). Complex thermoelectric materials. *Nature Materials*, *7*(2), 105–114. https://doi.org/10.1038/nmat2090

[33] Tang, J., & Skelton, J. M. (2021). Impact of noble-gas filler atoms on the lattice thermal conductivity of $CoSb_3$ skutterudites: First-principles modelling. *Journal of Physics: Condensed Matter*, *33*(16), 164002. https://doi.org/10.1088/1361-648X/abd8b8

[34] Nadtochiy, A., Kuryliuk, V., Strelchuk, V., Li, P., & Lee, S. (2019). Enhancing the Seebeck effect in Ge/Si through the combination of interfacial design features. *Scientific Reports*, *9*(1), 16335. https://doi.org/10.1038/s41598-019-52654-z

[35] Mao, T., Qiu, P., Hu, P., Du, X., Zhao, K., Wei, T., . . . , & Chen, L. (2020). Decoupling thermoelectric performance and stability in liquid-like thermoelectric materials. *Advanced Science*, *7*(1), 1901598. https://doi.org/10.1002/advs.201901598

[36] Muta, H., Kurosaki, K., & Yamanaka, S. (2004). Thermoelectric properties of doped $BaTiO_3$–$SrTiO_3$ solid solution. *Journal of Alloys and Compounds*, *368*(1–2), 22–24. https://doi.org/10.1016/j.jallcom.2003.07.016

[37] Yang, J. (2007). Foreword. *Journal of Electronic Materials*, *36*(7), 703. https://doi.org/10.1007/s11664-007-0179-4

How to Cite: Bhattacharjee, J., & Roy, S. (2026). Synthesis of Thermoelectric Nanocomposites by Incorporating Reduced Graphene Oxide. *Archives of Advanced Engineering Science*, *4*(2), 171–179. https://doi.org/10.47852/bonviewAAES42023514